Materials Today Chemistry 49 (2025) 103109

Contents lists available at ScienceDirect

Materials Today Chemistry

journal homepage: www.journals.elsevier.com/materials-today-chemistry/

Polymeric dye-loaded electrospun fibers for antimicrobial photodynamic therapy

Degnet Melese Dereje [a,b,1], Carlotta Pontremoli [a,*,1], Cristina Yus [c,d,e,**], Enrique Gámez [c,d,e], Monica Paesa [c,d,e], Gracia Mendoza [e], Manuel Arruebo [c,d,e], Nadia Barbero [a,f]

[a] Department of Chemistry, NIS Interdepartmental and INSTM Reference Centre, University of Torino, Via G. Quarello 15A, 10135, Torino, Italy
[b] Department of Chemical Engineering, Bahir Dar Institute of Technology, Bahir Dar University, Polypeda 01, 0026, Bahir Dar, Ethiopia
[c] Instituto de Nanociencia y Materiales de Aragón (INMA), CSIC-Universidad de Zaragoza, Zaragoza, 50009, Spain
[d] Department of Chemical Engineering. University of Zaragoza, Campus Río Ebro-Edificio I+D, C/ Poeta Mariano Esquillor S/N, 50018, Zaragoza, Spain
[e] Aragon Health Research Institute (IIS Aragon), 50009, Zaragoza, Spain
[f] Istituto di Scienza, Tecnologia e Sostenibilità per lo Sviluppo dei Materiali Ceramici (ISSMC-CNR), Faenza, RA, Italy

A B S T R A C T

As an alternative to the extensive use and misuse of antibiotics, antimicrobial photodynamic therapy stands out as a non-selective, broad-spectrum, locally and spatially controlled antimicrobial therapy. Reactive oxygen and nitrogen species, generated by appropriate light on specific photosensitizers in the presence of tissue oxygen, cause rapid bacterial damage with reduced chances for bacteria to develop adaptive mechanisms of acquired or genetic resistance. Herein, we developed a light-responsive advanced wound dressing based on electrospun polycaprolactone (PCL) nanofibers decorated with PLGA microparticles (MPs) encapsulating a polymethine cyanine dye (Br-CY5). This bilayer system was designed to enable bacterial inactivation upon light irradiation while providing sustained dye release and mechanical stability suited for chronic wound environments. The hybrid dressing was evaluated against *Staphylococcus aureus*, which is a bacterial pathogen commonly present on chronic infected wounds, addressing a 99.9 % reduction in the bacterial load after irradiating the dressing with a 640 nm LED for 15 min. Additionally, the cytotoxicity of the free dye and the developed dressing was assessed on various eukaryotic cell lines to ensure cytocompatibility. These results highlight the potential of this bilayered photodynamic system as an effective and safe antimicrobial wound dressing for managing chronic infections.

1. Introduction

Injuries resulting from burns, trauma, or surgical procedures not only exert a physical toll on individuals but also their care imposes a substantial economic and social burden on national healthcare systems. Acute wounds generally follow a well-orchestrated and efficient healing process, however a potential bacterial infection can introduce complexities, impeding the natural healing process and predisposing the wound to chronicity [1–3]. The conventional approach to mitigate the risk and impact of bacterial infections involves an initial wound cleansing and debridement followed by the extensive application of topical antiseptics or, in cases where the bone might be compromised (e.g., osteomyelitis, necrotizing fasciitis), antibiotics [4–6]. However, the rapid emergence of antibiotic-resistant strains of bacteria has prompted a judicious limitation for antibiotic use, emphasizing the importance of proper selection, dosage, and duration of treatments to prevent the development of resistance [2,6,7]. Antimicrobial resistance (AMR) stands as a formidable challenge to global public health, heralding a time when the once-powerful arsenal of conventional antibiotics is becoming progressively less effective, compromising the ability to combat bacterial infections and amplifying the number of untreatable diseases. According to the 2024 Lancet report [8], the global failure to tackle the problem of antibiotic resistance will globally cause an estimated 1.91 million deaths attributable to AMR and 8.22 million deaths associated with AMR in 2050, meaning that AMR will cause 39 million deaths between 2025 and 2050 – which equates to three deaths every minute.

As a proactive response to this urgent and escalating threat, researchers are fervently exploring alternative strategies that can circumvent the limitations of traditional antimicrobial agents. Among

This article is part of a special issue entitled: ICSM2024 published in Materials Today Chemistry.

* Corresponding author.
** Corresponding author. Instituto de Nanociencia y Materiales de Aragón (INMA), CSIC-Universidad de Zaragoza, Zaragoza, 50009, Spain.
E-mail addresses: carlotta.pontremoli@unito.it (C. Pontremoli), cyargon@unizar.es (C. Yus).

[1] These authors equally contributed to the manuscript.

https://doi.org/10.1016/j.mtchem.2025.103109
Received 18 March 2025; Received in revised form 22 September 2025; Accepted 6 October 2025
Available online 12 October 2025

these innovative approaches, Antimicrobial Photodynamic Therapy (aPDT) emerges as a promising avenue, showcasing the potential to revolutionize the landscape of infectious disease treatments [9–12]. The core of aPDT lies in a groundbreaking concept that harnesses the power of light in conjunction with a photosensitizer (PS). These PSs, when activated by specific light wavelengths, induce a cascade of reactions leading to the generation of singlet oxygen and/or reactive oxygen species (ROSs). Depending on the PS used, electron transfer processes trigger the production of superoxide anions and other reactive oxygen species ($^{\bullet}OH$, $O_2^{\bullet -}$, H_2O_2) (type I reactions) whereas energy transfer processes can produce singlet molecular oxygen ($^1O_2$) (type II reactions) [13]. This orchestrated process culminates in the selective inactivation of microbial pathogens. The advantage in the use of aPDT compared to conventional antibiotics is its ability to transcend the specificity limitations associated with traditional drugs. In fact, aPDT operates through a broader spectrum of activity, making it potentially effective against a diverse array of pathogens, including those that have developed resistance to conventional antibiotics. Systemic side effects are avoided due to its local application. ROS are very short lived species so, residual doses do not induce adaptation mechanisms on bacteria as antibiotics do. Having multiple mechanisms of antimicrobial action due to the non-selective oxidative stress generated by ROS, the chances for bacteria to develop resistance are minimized when using aPDT.

In this context, the choice of PSs becomes pivotal in determining the success of the therapy. Since the first use of eosin in 1904, various PSs were investigated, and within the last 20 years, several approaches were designed to optimize the photodynamic properties of PS by modifying the chemical structure or by developing new classes of PSs [13–15]. Among them, the phenothiazinium group, which includes methylene blue (MB) and toluidine blue O (TBO) are widely used in aPDT thanks to their cationic nature, able to bind both gram-negative and positive bacteria [15,16]. As an alternative, polymethine dyes (PMDs) such as cyanines (CYs) and squaraines (SQs) are known for their fluorescence and absorbance in the near-infrared window (also known as optical window or therapeutic window), which is broadly defined in biomedical PDT literature to include wavelengths starting around 640 nm and extending beyond 700 nm [17,18]. This classification is functionally relevant due to its tissue penetration and phototherapeutic applicability with a reduced autofluorescence compared to blue or green light. In fact, water and biological chromophores (*i.e.*, melanin, hemoglobin, etc.) show a minimal light absorption in that region and consequently light reaches deeper regions in the physiological tissues (compared to VIS light) [19,20]. This makes them ideal candidates for bioimaging and therapeutic applications, thanks to their extended conjugated system, resulting in unique optical properties with enhanced photostability, efficient singlet oxygen generation, and biocompatibility [13,21]. However, their tendency to self-aggregate in biological media can significantly affect their photochemical properties, detrimental in view of an efficient aPDT due to a reduction in the ROS generation capability. To overcome these drawbacks, a possible solution is the incorporation of these dyes inside drug delivery systems, allowing to prevent the formation of dye aggregates in physiological media and protect their photochemical characteristics [22–25]. For the effective management of infected wounds, a promising approach could be represented by the use of advanced wound dressings, which could play an important role during the healing process. In fact, ideal wound dressings containing antimicrobial compounds should protect the wound from physical damage and provide adequate gaseous exchange, absorb wound exudates, while reducing the bacterial bioburden on the wound bed [3,26].

In this context, electrospun fibers have gained significant attention in the field of biomedical applications, including both aPDT and wound healing. Electrospinning is a versatile technique that allows the production of nanofibrous materials with high surface area, porosity, and tunable properties, providing a high surface-to-volume ratio, thus facilitating the loading of large amounts of PSs within the fibers and also a better release and penetration of the PSs in the bacterial environment, aiding in their destruction after aPDT [26–28]. Compared with the use of the free PSs, electrospun PS-loaded dressings can act as controlled release systems with extended duration of action for the loaded PSs [29,30]. Also, the dressing itself acts as a protective barrier to prevent PS degradation from photobleaching and from the physiological pro-inflammatory oxidative environment generated after wounding. The exploration of incorporating dyes into electrospun fibers has been extensive, particularly utilizing a range of biodegradable and biocompatible polymers such as polycaprolactone (PCL), poly(lactic-co-glycolic acid) (PLGA), polylactic acid (PLA), and chitosan. Various commercial dyes like methylene blue, indocyanine green (ICG) and phthalocyanines have been loaded into these fibers for applications in aPDT and as potential regenerative medical devices with integrated aPDT capability [28,31]. For example, the combination of ICG and curcumin loaded into electrospun PLGA nanofibers has demonstrated a significant aPDT effect against both gram-positive and gram-negative bacteria [32]. Similarly, a curcumin-loaded PCL wound dressing showed aPDT efficacy in *in vivo* assays, leading to a notable decrease in the bacterial presence on infected mice wounds [33].

In the last few years, our group proposed different series of PMDs [34–36], among which different indolenine-based pentamethine cyanines were developed. Interestingly, a brominated CY5 (Br-CY5) showed proper photochemical properties, excellent ROS production ability, and PDT activity against MCF-7 tumour cell lines [36] and could be considered as a potential candidate for aPDT. The present work aims to develop a light responsive advanced wound dressing based on electrospun PCL fibers decorated with CY-loaded PLGA microparticles (MPs), able to inactivate bacteria after irradiation. Firstly, Br-CY5, COOH-CY5 (used as negative control) and toluidine blue O (as gold-standard molecule) (see structures in Fig. 1) were tested as aPDT PSs against representative gram-positive *Staphylococcus aureus* bacteria (*S. aureus*). To achieve a sustained release and preserve the photodynamic activity of the most promising molecule Br-CY5, the dye was encapsulated in PLGA microparticles and subsequently sprayed onto PCL nanofiber mats. This strategy was chosen because PCL, while mechanically robust and suitable for chronic wound environments [37,38], degrades very slowly and can limit dye diffusion and photodynamic efficacy due to its high crystallinity. In contrast, PLGA enables a faster degradation profile and facilitates both initial surface dye release and prolonged release from its internal network. This bilayer approach thus combines the advantages of both polymers to achieve a dressing capable of long-lasting antimicrobial action and mechanical resilience. Finally, the *in vitro* aPDT activity of the resulting electrospun fibers was evaluated.

2. Materials and methods

Polycaprolactone (PCL, Mn = 80,000 Da), phosphate buffered saline (PBS, 50 mM, pH 7.4) and toluidine Blue O were obtained from Sigma Aldrich (USA). PLGA (Resomer® RG 504) was obtained from Evonik Industries AG (Germany). Dichloromethane (DCM, >99 %), dimethyl sulfoxide (DMSO), *N,N*-dimethylformamide (DMF, >99 %) were obtained from Fisher Scientific (USA). All the chemicals were used without any further purification. GFP-expressing *S. aureus* strain, kindly donated by Dr. Iñigo Lasa (Universidad Pública de Navarra, Spain), was obtained using a pCN47 plasmid carrying a Phyper constitutive promoter as reporter of the GFP expression.

2.1. Synthesis of Br-CY5 and COOH-CY5

The typical synthesis of symmetrical pentamethine cyanine dyes involves the condensation of the quaternary heterocyclic salts bearing an activated methyl group, with a malonodialdehyde derivative. The synthetic procedure followed to prepare the Br-CY5 and COOH-CY5 has been described in Pontremoli *et al.* [36]. The characterization of the final Br-CY5 and COOH-CY5 as well as all the intermediate compounds agree with literature values [35,36].

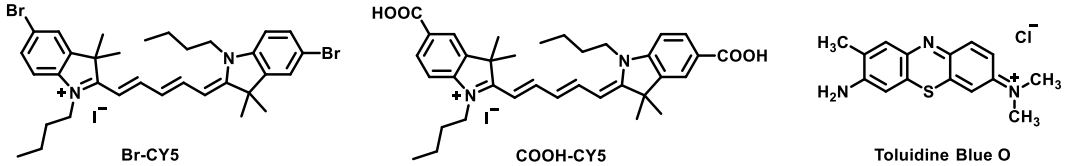

Fig. 1. Molecular structure of the selected dyes.

2.2. Evaluation of the reactive oxygen species (ROS) generation

To evaluate ROS generation, three different scavenger molecules were used as probes to detect generated ROS. Firstly, 1,3-Diphenylisobenzofuran (DPBF) (>97 %, Sigma Aldrich) was selected by following the protocol previously described in the literature [22,34,36]. Stock solutions of DPBF [740 μM], Br-CY5 and COOH-CY [350 μM] were prepared in DMSO, while the stock solution of toluidine [350 μM] was prepared directly in PBS. Each solution was then diluted in PBS to obtain the final desired concentration (25 μM for DPBF, 5 μM for cyanines and toluidine) placed in a 1 cm quartz cell and irradiated in an aerated solar box (Solarbox 3000e, 250 W xenon lamp, CO.FO.ME.GRA) at various time intervals. Light was filtered through an optical filter with a 515 nm cut-off, to avoid DPBF degradation. At predefined time points, absorption spectra were recorded on a Cary 300 Bio spectrophotometer (Varian, Santa Clara, CA, USA). Measurements were conducted within the 300–600 nm range at room temperature using quartz cuvettes with a 1 cm pathway length. The decrease in the DPBF absorption contribution at 415 nm was plotted as a function of the irradiation time.

DCFH was employed as second probe to evaluate the ROS production of the dyes, by following the procedures reported in the literature [39,40]. 2′,7′-Dichlorofluorescein (DCFH) is a nonfluorescent compound that after oxidation produces 2′,7′-dichlorofluorescein (DCF), a strong fluorescent molecule. DCFH was prepared starting from DCFH-DA (2′,7′-Dichlorofluorescein diacetate, Calbiochem) by mixing 0.5 mL of 1.0 mM DCFH-DA in methanol with 2.0 mL of 0.01 N NaOH, at room temperature for 30 min. After the reaction time, the mixture pH was neutralized at pH 7.4 by using 10 mL of 25 mM NaH_2PO_4. This solution was stored in a freezer and protected from the light until further use. The $^1O_2$ scavenger activity can be monitored through an increase in the emission fluorescence of DCF at 520 nm, using the excitation wavelength of 495 nm.

All the measurements were performed in a total volume of 3.0 mL of phosphate buffer (10 mM, pH 7.4), containing 1 μL of DCFH solution and SQ (0.5 μM). Each solution was placed in a 1 cm quartz cell and irradiated at different time points under stirring in an aerated solar box (Solarbox 3000e, 250 W xenon lamp, CO.FO.ME.GRA) with a 250 W lamp. Light was filtered in an optical filter with a 515 nm cut-off, to avoid DCFH degradation.

At predefined time points (30, 60, 90, 120, 240 and 300 s), fluorescence emission spectra were recorded by using a Horiba Jobin Yvon Fluorolog 3 TCSPC fluorimeter. The increase in the DCF fluorescence emission at 520 nm was finally plotted as a function of the irradiation time.

A third protocol was assessed to confirm if the ROS production capacity of Br-CY5 was maintained when in contact with *S. aureus* by using the oxidation sensitive probe dihydrorhodamine 123 (DHR 123, Sigma-Aldrich, USA), modifying the protocol reported in the literature [39]. Briefly, a 10^9 Colony Forming Units per mL (CFU/mL) stock dispersion of *S. aureus* was prepared in PBS and a 400 μM stock solution of Br-CY5 was prepared in DMSO. Then, both stock solutions were diluted in PBS at the final concentration of 1×10^5 CFU/mL of *S. aureus* and 100, 200 and 400 nM of Br-CY5 and mixed in P96 well plates. A stock solution of DHR 123 was prepared in DMSO and diluted in PBS at pH 7.4 to obtain a final concentration of 40 μM. After 1 h of incubation, the solution of DHR 123 in PBS was added into each well and irradiated with a compact RED-LED array-based illumination system specifically designed and produced by Cicci Research s.r.l (Italy). This illumination system includes a RED-LED array (light source with excitation wavelength: 640 nm) composed of 96 LEDs arranged in 12 columns x 8 rows. The irradiance was set at 5.5 mW/cm^2. At predefined time points (15, 30, 45 and 60 min), the fluorescence of each well was recorded with a Varioskan LUX multimode microplate reader (Thermo Fisher Scientific, USA) in order to evaluate the increase in the DHR 123 emission contribution at 530 nm (excitation wavelength 488 nm) characteristic of the ROS generated. The increase in the DHR 123 emission was then plotted as a function of the irradiation time. The obtained values were compared with an untreated solution of 10^5 CFU/mL of *S. aureus*, used as a negative control. Moreover, the same experiment was conducted in the absence of *S. aureus,* replacing bacteria with PBS, in order to investigate if the ROS production of Br-CY5 was affected by the presence of *S. aureus*.

All measurements were performed in triplicate starting from different stock solutions and plotted as averages with the corresponding standard deviations.

2.3. Effect of the time and irradiation power on the temperature

In order to investigate the effect of different irradiation times and power on bacterial inactivation, a preliminary temperature evaluation test was conducted to confirm that the bacterial inactivation was caused by the photodynamic effect induced by the presence of the PS and not by a photothermal effect. For this purpose, Br-CY5 was first dissolved in DMSO and then appropriately diluted in PBS to obtain different concentrations of 100, 200 and 400 nM (total amount of DMSO <1 %). Then, solutions of Br-CY5 were placed in P96 well plates and irradiated by using a compact RED-LED array-based illumination system (Cicci Research s.r.l, Italy), using an irradiance of 5.5, 7, and 17.4 mW/cm^2 up to 120 min. A thermocouple was immersed in each well in order to evaluate the potential increase in the temperature during the experiment. Moreover, the same experiment was conducted in the absence of Br-CY5 (using PBS, as a reference).

2.4. Evaluation of the Br-CY5 photodegradation

A stock solution of Br-CY5 was prepared in DMSO and diluted in PBS at the final concentration of 44 μM in P96 well plates and irradiated with a compact LED array-based illumination system (Cicci Research s.r.l, Italy). The irradiance was set at 5.5 mW/cm^2. At predefined time points (1, 3 and 8 min), the absorbance of the Br-CY5 was recorded by using a Varioskan LUX multimode microplate reader in the range of 500–800 nm at room temperature. The Br-CY5 photodegradation was evaluated by following the decrease in the absorbance at 650 nm as a function of the irradiation time.

2.5. Preparation of electrospun PCL nanofibers decorated with empty PLGA MPs and Br-CY5-loaded PLGA MPs

Electrospun PCL fibers were firstly prepared by following the protocol previously reported in the literature [3,40] using a Professional LabDevice electrospinner (Doxa Microfluidics, Spain) equipped with an 8 cm aluminum disc collector covered with aluminum foil and a needle (inner diameter, 0.6 mm) as injector. Collector and injector were connected to a negative and a positive high voltage source, respectively.

A solution of PCL (10 % w/w) in a mixture of DCM and DMF (1:1 v/v)

was prepared and stirred at room temperature overnight. The solution was transferred to a 10 mL syringe, sonicated to remove air bubbles, and connected to the injector. The distance between injector and collector was set at 18 cm, the flow rate was set at 1 mL/h and voltages were set at +7.2 and −4.1 kV for the injector and the collector, respectively. A 2D motion module was applied for 2 h to obtain a homogeneous electrospun mat.

For the decoration of the previously formed PCL mats with PLGA MPs, a previously reported protocol was adapted [3]. Briefly, a PLGA solution (10 % w/w) in DMF was prepared. For Br-CY5 loaded MPs, a dye solution (10 mg/mL) in DCM was added to the PLGA solution to reach a final dye concentration of 0.5 mg/mL. This concentration was selected using toluidine as a dye model due to the availability of this commercial dye. When the toluidine concentration was above 0.5 mg/mL, significant instability impaired the electrospraying process. Without removing the previously prepared PCL fiber mat from the collector, the injector to collector distance was changed to 30 cm, the flow rate was set at 0.5 mL/h and voltages were adjusted to +11.6 and −4.1 kV for empty PLGA MPs and +14.3 and −4.4 kV for Br-CY5 loaded MPs, in order to obtain a stable Taylor's cone (Table 1). A 2D motion module was applied for 4 h to uniformly cover the previously obtained PCL mat with the electrosprayed dye-loaded PLGA MPs. Samples were named as PLGA-PCL for PCL mats decorated with bare PLGA MPs and Br-CY5@PLGA-PCL for PCL mats decorated with Br-CY5 loaded PLGA MPs.

2.6. Characterization of the electrospun PCL nanofibers decorated with empty PLGA MPs and Br-CY5-loaded PLGA MPs

Scanning Electron Microscopy (SEM). The morphology of the bare PCL fibers, PLGA-PCL and Br-CY5@PLGA-PCL was evaluated by SEM using an Inspect F-50 microscope (FEI Company, Netherlands). For the SEM observations, fibers were attached with conductive carbon tape to a microscope sample holder and coated with a Pd layer (5 nm). The fibers thickness as well as the PLGA MPs diameters were measured using ImageJ software (N = 100).

Entrapment Efficiency (EE%) and drug loading content (LC%) evaluation. The amount of dye loaded in the electrospun Br-CY5@PLGA-PCL was calculated by a direct method using UV–Vis spectroscopy. A calibration curve of free Br-CY5 in DMSO (at the absorption wavelength of 652 nm) was prepared as previously reported by the authors [36]. Then, 5 mg of electrospun Br-CY5@PLGA-PCL were dissolved in DMSO and sonicated for 5 min to facilitate the dissolution of the MPs and the release of the encapsulated dye to the solution. The latter was then analyzed by UV–Vis in a Varioskan LUX multimode microplate reader and by using the Beer-Lambert equation (molar extinction coefficient, ε, of Br-CY5 = 265,000 $M^{-1}cm^{-1}$) the concentration of the released dye was calculated. The final entrapment efficiency as well as the drug loading content were calculated according to the standard equations (1) and (2) [41]:

$$\text{Entrapment Efficacy EE}\,(\%) = \frac{mg\ of\ released\ Br-CY5}{mg\ of\ initial\ weighted\ Br-Cy5} \cdot 100 \quad (1)$$

$$\text{Drug Loading Capacity LC}\,(\%) = \frac{mass\ of\ Br-CY5\ (encapsulated)}{mass\ of\ Br-CY5@PLGA-PCL\ fibers} \cdot 100 \quad (2)$$

2.7. Drug release studies from Br-CY5@PLGA-PCL fibers

Drug release studies were carried out in PBS supplemented with Tween-20 at 2 % v/v (in order to mimic the effect of amphiphilic compounds present in culture media). Some membranes of Br-CY5@PLGA-PCL fibers were cut and incubated in the release medium at 37 °C under agitation (150 rpm) for different times (0, 1, 2, 4, 6 and 24 h) under sink conditions. At each time point, the corresponding membrane was removed and Br-CY5 absorbance (650 nm) was measured in a Varioskan LUX multimode microplate reader. Br-CY5 concentration was obtained by interpolation with a calibration curve derived from different Br-CY5 solutions of known concentrations in the release medium. To gain a deeper understanding of the release mechanisms of the dye, the Korsmeyer–Peppas equation [42] was applied to estimate the release exponent *n*. This parameter helps classify the type of release mechanism. Specifically, an *n* value lower or corresponding to 0.45 indicates diffusion-controlled release, values of *n* between 0.45 and 0.89 denote an anomalous (non-Fickian) release while a value of 0.89 suggests swelling or relaxation-controlled release, whereas *n* values exceeding 0.89 imply the involvement of additional mechanisms beyond diffusion and swelling/relaxation. Experiments were conducted in triplicate, with one membrane for each time point and three replicas.

2.8. In vitro bacterial assay for evaluating planktonic growth inhibition

GFP expressing *S. aureus* strain was selected to evaluate the antimicrobial properties of Br-CY5, COOH-CY5, toluidine and electrospun Br-CY5@PLGA-PCL systems before and after irradiation.

To initiate the bacterial culture, a colony of the bacterium was cultured in 4 mL of TSB at 37 °C under stirring conditions (150 rpm) overnight. The bacterial culture was centrifuged (1500 rpm for 5 min) and the pellet was washed with PBS (to remove TSB) and finally diluted with PBS to obtain a concentration of 10^8 CFU/mL.

Due to their hydrophobic nature Br-CY5 and COOH-CY5 were firstly dissolved in DMSO and then appropriately diluted in PBS to obtain different concentrations of the samples with a total amount of DMSO less than 1 %, while toluidine was directly solubilized in PBS and diluted to the desired concentrations. Then, 20 μL of Br-CY5, COOH-CY5 and toluidine solutions were placed in contact in a P96 well plate with 180 μL of the prepared *S. aureus* inoculum to obtain the final concentration of 100, 200, and 400 nM for Br-CY5, COOH-CY5 and toluidine. Additionally, final concentrations of 1, 5, and 10 μM for toluidine were also tested, according to the amounts usually employed in the literature [43, 44].

The culture was incubated at 37 °C and under stirring conditions (150 rpm) for 120 min to allow the dye to diffuse. Irradiation (λ = 640 nm) was then carried out by using the compact RED-LED array-based illumination system previously mentioned. For standard treatments, the following parameters were used: 15 min of irradiation, (irradiance 5.5 mW/cm^2, fluence 5 J/cm^2). Other experiments were performed maintaining the irradiance at 5.5 mW/cm^2, increasing the irradiation time: 30 min (fluence 9.9 J/cm^2), 45 min (fluence 14.85 J/cm^2) and 60 min (fluence 19.8 J/cm^2) or increasing both the irradiance at 7 mW/cm^2 and the irradiation time: 15 min (fluence 6.2 J/cm^2), 30 min (fluence 12.6 J/cm^2), 45 min (fluence 18.9 J/cm^2) and 60 min (fluence 25.2 J/cm^2). After 1 h of incubation, viable bacteria were quantified by the serial dilution method. To evaluate the potential dark toxicity, the same experiments were performed maintaining the samples in the dark. Each experimental condition was performed in duplicate in three

Table 1
Parameters for the preparation of the PLGA-PCL fibers and Br-CY5@PLGA-PCL fiber using electrospinning. "RH" stands for relative humidity and "HV" stands for high voltage.

Samples	Temp. [°C]	RH [%]	HV injector [kV]	HV collector [kV]	PCL-solution flow rate [mL/h]	PLGA-solution flow rate [mL/h]
PLGA-PCL	28	19.3	+11.66	−4.1	1.0	0.5
Br-CY5@PLGA-PCL	29	15.6	+14.3	−4.4	1.0	0.5

independent experiments.

The same experimental setup was maintained for the evaluation of the antimicrobial activity of the electrospun Br-CY5@PLGA-PCL system, by analyzing a piece of the fibers containing the highest concentration of tested free Br-CY5 (*i.e.*, 400 nM) and evaluating also the 800 nM concentration irradiated after an incubation of 1 and 24 h with bacteria.

2.9. Confocal analysis

In order to study bacterial adhesion to the synthesized electrospun systems, the intrinsic fluorescence of the GFP protein expressed by the *S. aureus* bacterial strain and the fluorescence of the Br-CY5 incorporated into the MPs were both utilized. To visualize dead bacteria, the samples were stained with propidium iodide (PI). After 1 h of incubation of bacteria with the decorated fibers, those were fixed by incubation in a 4 % v/v paraformaldehyde in PBS solution for 45 min. Subsequently, samples were washed with PBS and incubated in a 10 μM PI solution for 30 min, followed by another PBS wash to remove the excess of PI in the samples before preparing them for visualization. This entire process was performed in the dark to prevent Br-CY5 and PI degradation. For the irradiated samples, the mats where irradiated at 17.4 mW/cm^2 for 15 min before fixation. Samples were visualized by using a confocal microscope (Confocal Zeiss LSM 880, Zeiss, Germany).

2.10. In vitro cytotoxicity assay

The cytotoxicity of the Br-CY5 PS and the Br-CY5@PLGA-PCL systems was evaluated in a 2D model with three different cellular lines: human dermal fibroblasts (NHDF-Ad, Lonza, Belgium), keratinocytes (HaCaT, kindly donated by Dr. Pilar Martin-Duque) and J774A.1 macrophages (ATCC-TIB-67™, LGC Standards, Spain). All cell lines were cultured in high-glucose Dulbecco's modified Eagle's medium (DMEM w/stable glutamine, Biowest, France) supplemented with 1 % (v/v) antibiotic-antimycotic solution (PSA, Biowest, France), and 10 % (v/v) fetal bovine serum (FBS, Gibco, USA) in a 5 % CO_2 atmosphere at 37 °C.

Fibroblasts, macrophages and HaCaT cells were seeded in P96 well plates and cultured for 24 h to ensure the adhesion of cells to the bottom of the wells. Then, the culture medium was replaced with fresh medium containing the tested concentrations of Br-CY5 and the pre-weighed fragments of the Br-CY5@PCL-PLGA system. The PCL-PLGA system was also assayed to ensure the cytocompatibility of the polymers without the PS. After 24 h cytotoxicity was evaluated by measuring cell metabolism with the Blue Cell Viability assay (Abnova, Taiwan) following the manufacturer's instructions. Cells were incubated with the reagent (10 % v/v in DMEM) for 4 h (37 °C and 5 % CO_2 atmosphere) and the fluorescence was read ($\lambda_{ex}/\lambda_{em}$ 530/590 nm) in a Varioskan LUX multimode microplate reader. Viability was determined by interpolation, considering 100 % of cellular viability the fluorescence of untreated cells.

Three experiments with 4 replicas were performed to obtain results as mean ± SD.

2.11. Statistical study

Data were reported as an average of 3 independent experiments with the corresponding standard deviations (SD). Statistical analyses were performed using the two-tailed Student's t-test (Excel, Microsoft Office Professional Plus 2016) to determine the difference between the two groups (dark *vs.* light). Differences with a *p*-values (p) < 0.05 were considered statistically significant and represented as follows *: $p < 0.05$; **: $p < 0.01$; ***: $p < 0.001$; ****: $p < 0.0001$. Concerning the *in vitro* cytotoxicity tests, data were analyzed using GraphPad Prism 8 (GraphPad Software Inc., USA) by two-way ANOVA followed by multiple comparison tests. Statistical significance was defined as follows: *$p < 0.05$, **$p < 0.01$, ***$p < 0.001$, and ****$p < 0.0001$, comparing untreated control cells with treated cells.

3. Results and discussion

3.1. Evaluation of the ROS by using DPBF and DCHF as probes

To fully compare the photodynamic response of the three dyes, a preliminary assessment of the ROS production ability of the three PSs under study was conducted using both DPBF and DCHF as probes by monitoring the absorbance decay at 415 nm and the emission increase at 520 nm, respectively, under simulated sunlight exposure. COOH-CY5 was used as a negative control due to its lack of significant ROS production [36], while, as we mentioned before, toluidine, a well-established photosensitizer, served as a literature standard known for its antimicrobial properties. As previously reported [36] and described in Fig. S1A, the COOH-CY5 sample showed negligible DPBF decay, as well as toluidine which showed just a moderate decay. Br-CY5 showed the highest rate of DPBF decay, indicating significantly greater ROS generation than both toluidine and COOH-CY5.

To confirm the ROS production trends observed with DPBF, additional measurements were performed using DCHF as an alternative ROS probe. As shown in Fig. S1B, the fluorescence intensity at 520 nm increased minimally for COOH-CY5, confirming its negligible ROS generation. Toluidine displayed a moderate fluorescence increase, consistent with its known photosensitizing properties. In contrast, Br-CY5 induced the most pronounced fluorescence enhancement, further supporting its superior ROS production capacity under simulated sunlight exposure. These results are in agreement with those obtained using DPBF, reinforcing the higher photodynamic efficiency of Br-CY5 compared to the other compounds tested. These overall results suggest that Br-CY5 could be a promising candidate for applications requiring high ROS generation, such as antimicrobial treatments.

3.2. In vitro bacterial evaluation of free PS for planktonic growth inhibition

Once assessed the ROS production capability, Br-CY5, COOH-CY5 and toluidine were tested against GFP expressing *S. aureus* bacteria to evaluate aPDT activity. Initially, aPDT treatment parameters were selected based on previous studies [22,36,45]. These parameters included dye concentrations of 100, 200 and 400 nM in 1 × PBS buffer at pH 7.4, an irradiation time of 15 min, fluence of 5 J/cm^2, and irradiance of 5.5 mW/cm^2. All samples exhibited no toxicity under dark conditions. When irradiated, Br-CY5 showed a substantial bacterial eradication with an approximately 2-log reduction of bacteria viability at all the tested concentrations (Fig. 2A). On the other hand, both COOH-CY5 and toluidine did not demonstrate any aPDT activity at those concentrations (Fig. 2B and C, respectively). The behavior observed for COOH-CY5 was presumably expected, due to its low ROS production as already observed against cancer cells [36]. Concerning toluidine, the literature reported that the concentration useful to inactivate bacteria is generally above 5 μM [46,47]. Therefore, we observed that by increasing the toluidine concentration up to 10 μM, a large bacterial eradication was observed, with a 2.5-log reduction at 5 μM and a complete bacteria elimination at 10 μM (Fig. 2D).

As reported in Fig. 2A, the reduction in bacteria viability induced by Br-CY5 was not dependent on the concentration. To further investigate this behavior, we decided to evaluate the ROS production of the Br-CY5 at different concentrations when in contact with *S. aureus*, following a protocol that better mimics the antimicrobial PDT environment, by using the oxidation-sensitive probe DHR 123. The difference in ROS production at each concentration between the dye alone in PBS and when in contact with bacteria was found to be negligible (Fig. 2E and F, respectively). Irrespective of the concentration tested, the ROS production increased during the first 45 min, reaching a plateau. Notably, the presence of bacteria in contact with the dye did not significantly affect its ROS production.

Based on these considerations, we decided to investigate the aPDT

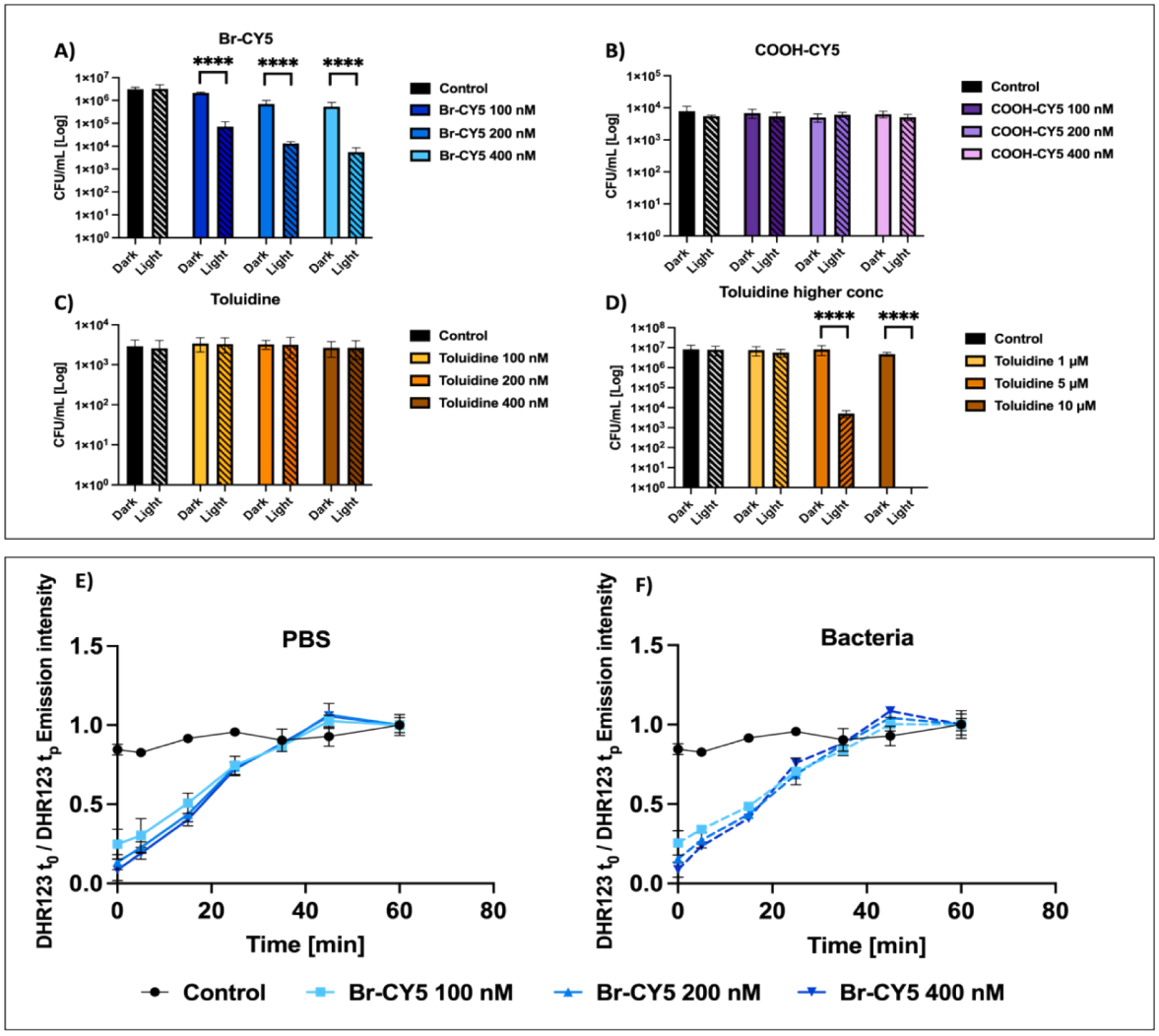

Fig. 2. *In vitro* antimicrobial effect of different concentrations of A) Br-CY5 at 100, 200 and 400 nM, B) COOH-CY5 at 100, 200 and 400 nM, C) Toluidine at 100, 200 and 400 nM and D) Toluidine at 1, 5 and 10 μM against *S. aureus* (640 nm LED, irradiation time 15 min, fluence of 5 J/cm^2, and irradiance of 5.5 mW/cm^2). Each experimental condition was performed in duplicate in three independent experiments. Statistical analyses were performed using the two-tailed Student's t-test (Excel, Microsoft Office Professional Plus 2016) to determine the difference between the two groups (dark vs. light). Differences with a *p*-values (p) < 0.05 were considered statistically significant and represented as follows *: $p < 0.05$; **: $p < 0.01$; ***: $p < 0.001$; ****: $p < 0.0001$.
ROS production of Br-CY5 dye in PBS (E) and in contact with *S. aureus* (F) using DHR 123 (640 nm LED irradiance of 5.5 mW/cm^2). All measurements were performed in triplicate starting from different stock solutions and plotted as averages with the corresponding standard deviations.

effect of Br-CY5 by increasing both irradiation time and power. However, the increase in power and irradiation time could lead to an unwanted increase in temperature, potentially causing bacterial death (due to a photothermal effect and not due to a photodynamic one). Thus, before proceeding with the antibacterial test, an additional experiment was carried out to measure the kinetic increase in temperature under the presence of different concentrations of Br-CY5 (100, 200 and 400 nM) as a function of time (up to 2 h) with three selected irradiances (5.5, 7 and 17.4 mW/cm^2). As reported in Figs. S2A, S2B, and S2C irrespective of the irradiance selected, the temperature slightly increased from ~25 to ~30 °C during the first hour of irradiation and then reaching a plateau until the maximum time evaluated (2 h). The same behavior was also observed for the samples just treated with PBS as control. These results confirm that the LED irradiation used, in the presence of Br-CY5, does not induce a sufficient temperature increase to cause bacterial death and the bacterial eradication observed was due a photodynamic effect solely.

Once assessed that the irradiation did not induce a relevant temperature increase, the antimicrobial assay was performed, by setting the different parameters reported in Table 2.

Table 2
Parameters used for the aPDT treatments against *S. aureus*.

Irradiance (mW/cm^2)	Fluence (J/cm^2)			
	15 min	30 min	45 min	60 min
5.5	5	9.9	14.8	19.8
7	6.3	12.6	18.9	25.2
17.4	15.8	31.3	46.8	62.6

Fig. 3A, B and 3C report the antibacterial activity of different concentrations of Br-CY5 under different irradiations over time. Specifically, Fig. 3A shows the response in terms of bacterial counts for Br-CY5 irradiated at 5.5 mW/cm^2. As previously observed (Fig. 2A), no significant decrease in bacterial counts was evident in dark conditions for any of the concentrations tested. After irradiation, a significant reduction in bacterial counts could be observed. Nonetheless, the decrease in bacterial count was not proportional to either dye concentration or irradiation time.

When the irradiance was increased to 7 (Figs. 3B) and 17.4 mW/cm^2

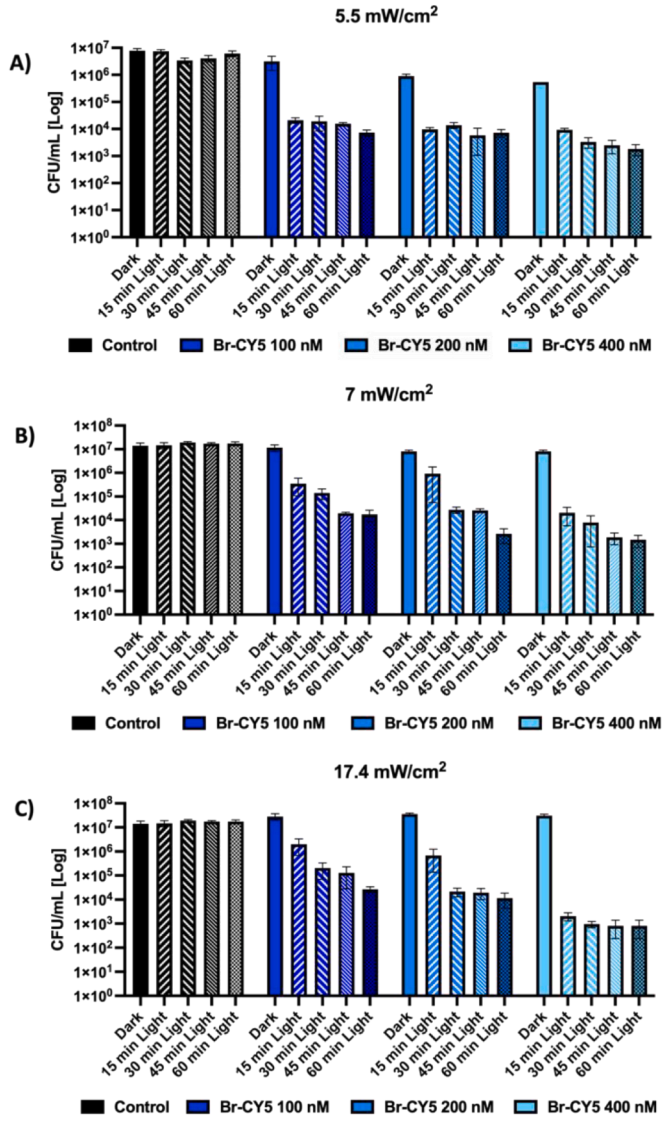

Fig. 3. *In vitro* antimicrobial effect of Br-CY5 against *S. aureus* bacteria at concentrations of 100, 200, and 400 nM, and irradiation times of 15, 30, 45, and 60 min (640 nm LED, Irradiance of A) 5.5 mW/cm^2, B) 7 mW/cm^2 and C) 17.4 mW/cm^2. Each experimental condition was performed in duplicate in three independent experiments.

(Fig. 3C), a greater effect of both concentration and irradiation time was observed, with a significant reduction in bacterial counts especially when irradiated at 17.4 mW/cm^2 at a concentration of 400 nM (up to approximately 4-log reduction). However, it is also evident that increasing the irradiation time for Br-CY5 at 400 nM using 17.4 mW/cm^2 irradiance did not result in a proportional decrease in bacterial viability, instead a plateau in the reduction of bacteria viability was observed. To further investigate this phenomenon, we decided to evaluate the photostability of the molecule under different irradiations. As shown in Fig. S3, the dye exhibited photodegradation already when irradiated at 5.5 mW/cm^2. Specifically, after 8 min of irradiation, the absorption peak decreases by 70 %, highlighting that the photosensitizer is probably uncapable to produce ROS. Thus, to protect the dye from the photodegradation, Br-CY5 was incorporated into PLGA MPs which were subsequently deposited on the electrospun PCL mats.

3.3. Preparation and physicochemical characterization of electrospun PCL nanofibers decorated with Br-CY5-loaded PLGA MPs

To be potentially used as wound dressings, Br-CY5 loaded PLGA MPs were electrosprayed onto the PCL mats previously prepared by electrospinning, as reported in the experimental section. For comparison, PCL mats decorated with empty (*i.e.*, lacking Br-CY5) PLGA MPs were also prepared.

Morphological analysis was performed by SEM; for both the mats decorated with empty and Br-CY5 loaded PLGA MPs. On the bottom part, PCL mats revealed that nanofibers present high porosity, high tortuosity and a homogeneous diameter of 1.03 ± 0.2 μm (Fig. 4A and S4A). On the top side, electrosprayed PLGA MPs showed a spherical morphology and a uniform distribution, with a diameter of 0.80 ± 0.21 μm (Fig. 4B and S4B). As evidenced in Fig. 4A despite the high porosity of the mats, MPs did not percolate through them, being only present on their top part, consistent with our previous work [3]. The loading of the Br-CY5 into the PGLA MPs did not modify the morphology of the particles, while a slight increase in their sizes can be observed, with a diameter of 1 ± 0.2 μm, as is shown in Fig. 4C and D, S4C and S4D. The encapsulation efficiency of Br-CY5 in Br-CY5@PLGA-PCL was 57 wt%, with a loading content of 0.12 wt%.

3.4. In vitro bacterial assay of Br-CY5@PLGA-PCL system

The photodynamic effect of the Br-CY5@PLGA-PCL against Gram-positive *S. aureus* was investigated using the parameters described in Table 2, irradiating for 15 min and incubating the samples for 1 and 24 h. Concerning the samples incubated for 1h, as reported in Fig. 4E, by using an irradiance of 5.5 mW/cm^2, no bacterial inactivation was observed even at high concentrations (up to 800 nM). By increasing the irradiance to 7 mW/cm^2, 1-log reduction was evident only at 800 nM dye concentration. On the contrary, 2-log reduction was obtained when irradiating at 17.4 mW/cm^2, when working with 800 nM concentration. This decrease in the aPDT effect, compared to the free dye (see Fig. 3A–C), can be ascribed to the influence of the PLGA polymeric matrix. In fact, the presence of the polymeric matrix can scatter the incident light, decreasing the light dose able to excite the loaded cyanine dye [23]. Moreover, this experiment was performed just after 1 h of incubation of the system with bacteria. This time did not allow a substantial release of the dye as shown in Fig. 4F. In the first hour of incubation just about 5 % of the dye was released, probably corresponding to the dissolution and the fast diffusion of the dye from the outermost part of the particles in contact with the aqueous release medium. The release kinetics of Br-CY5 could be probably ascribed to its reduced aqueous solubility in aqueous buffer as well as to the slow erosion/swelling of the PLGA MPs (i.e., a complete matrix erosion is reached after 3 months for Resomer® RG 504, according to the manufacturer). To clarify the dye release mechanism, the equation of Korsmeyer-Peppas was employed to estimate the release exponent *n*. Br-CY5 delivery from PLGA microparticles turned out to be a purely Fickian diffusion-driven release, with an n exponent of 0.2. This suggests that the release is predominantly governed by passive diffusion through the polymer matrix, confirming the minimal contribution from polymer relaxation or erosion processes within the studied timeframe. Based on these considerations, the antimicrobial activity studies of Br-CY5@PLGA-PCL were also conducted after incubating the membranes with bacteria for 24 h. In Fig. 4E, a 1-log bacterial reduction was observed upon irradiation for 15 min at 5.5 mW/cm^2, at both 400 and 800 nM concentrations. The same behaviour can be observed increasing the irradiance to 7 mW/cm^2, which led to a 1-log reduction for the 400 nM of encapsulated Br-CY5 dye, and to a 1.5-log reduction was achieved when using the 800 nM one. Finally, the irradiation by using an irradiance of 17.4 mW/cm^2 for 15 min resulted in a 3-log reduction for both concentrations. These results indicate that the photodynamic antibacterial activity of the encapsulated dye is less effective compared to that

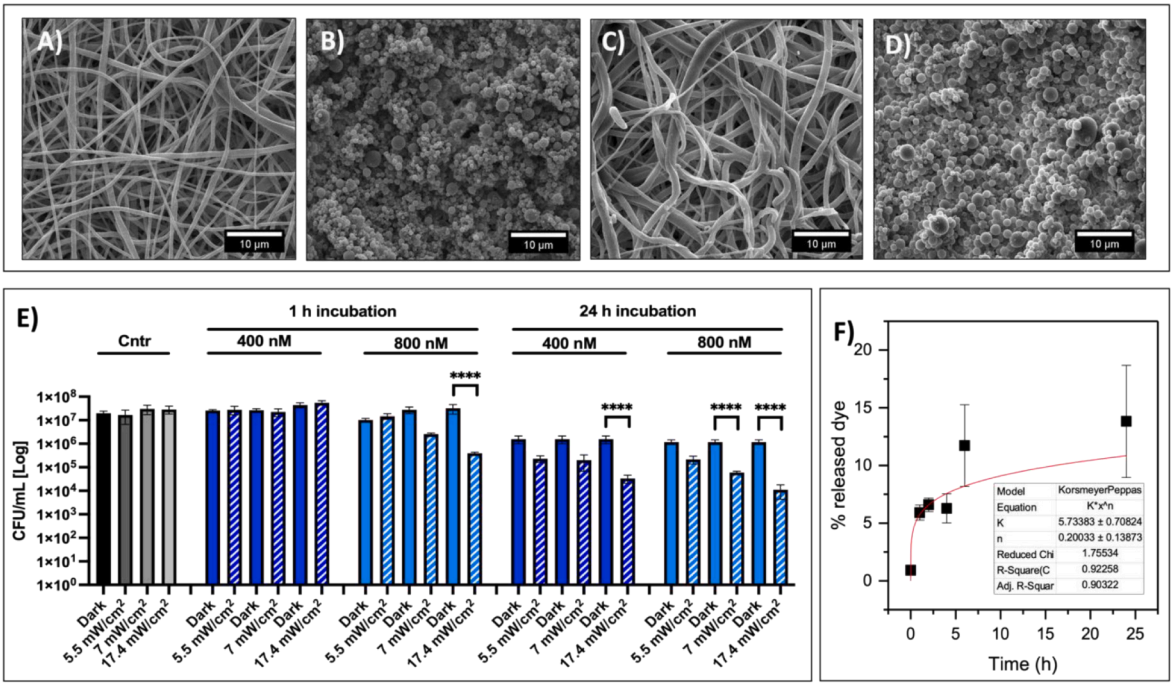

Fig. 4. SEM images of A) bottom side of PCL fibers decorated with empty PLGA MPs; B) top side of the mats having electrosprayed empty PLGA MPs; C) bottom side of PCL fibers decorated with Br-CY5 loaded PLGA MPs; D) top side of the mats having Br-CY5 loaded PLGA MPs. E) *In vitro* antimicrobial effect of Br-CY5@PLGA-PCL after 1and 24 h of incubation against *S. aureus* bacteria at concentrations of 400 and 800 nM after 15 min of irradiation using 640 nm LED and irradiances of 5.5, 7 and 17.4 mW/cm^2. Each experimental condition was performed in duplicate in three independent experiments. Statistical analyses were performed using the two-tailed Student's t-test (Excel, Microsoft Office Professional Plus 2016) to determine the difference between the two groups (dark vs. light). Differences with a p-values (p) < 0.05 were considered statistically significant and represented as follows *: $p < 0.05$; **: $p < 0.01$; ***: $p < 0.001$; ****: $p < 0.0001$. F) Release profile of Br-CY5 from Br-CY5@PLGA-PCL system. Measurements were performed in triplicate starting from different stock solutions and plotted as averages with the corresponding standard deviations.

for the free dye, which achieved a 4-log bacterial viability reduction at 400 nM at 17.4 mW/cm^2. However, encapsulation provides photoprotection, allowing the dye to maintain its photodynamic activity even after 24 h of incubation and resulting in an extended duration of its antimicrobial action, which represents a very positive outcome.

3.5. Confocal fluorescent microscopy analysis

In order to visualize the detailed information about the spatial distribution and dynamics of the antimicrobial photodynamic effect upon light irradiation, we performed confocal fluorescent microscopy. As shown in Fig. 5, confocal microscopy revealed the successful encapsulation of Br-CY5 within the PLGA MPs (blue channel) and the GFP expressed by viable bacteria (green channel). When bacteria die, their membrane becomes permeable, allowing PI to penetrate and stain the bacteria by binding to their intracellular DNA (red channel). As depicted in Fig. 5A, when fluorescent *S. aureus* bacteria were incubated with Br-CY5@PLGA-PCL mats but not irradiated, no dead bacteria were observed, as only fluorescent spots were seen in the green channel, and no fluorescent signal was observed in the red channel. However, when samples were irradiated at 17.4 mW/cm^2, the bacteria began to die, as evidenced by the appearance of the red PI signals in the images. Additionally, the orthogonal 3D projections displayed in Fig. 5B, showed that the bacteria were located on the outermost layer of the mat without penetrating it. Therefore, Br-CY5@PLGA-PCL mats can be effectively used also as prophylactic barriers, preventing the re-infection of the treated wounds, as bacteria are unable to traverse them.

3.6. In vitro cytotoxicity of Br-CY5@PLGA-PCL

Finally, we evaluated the *in vitro* cytotoxicity of the Br-CY5@PLGA-PCL fibers against epithelial and immune cells. In previous studies, it was found that Br-CY5 was cytotoxic against tumoral cells at concentrations higher than 200 nM [36]. This concentration is considerably lower than the Br-CY5 concentration encapsulated in the material synthetized in this work but in this device the released dye exhibits bactericidal activity against *S. aureus* and no cytotoxic effect against epithelial and immune cells attributed to the sustained release to the medium. It has been previously reported that the encapsulation of PSs in polymeric matrices could reduce their toxicity [3,48–50]. We assessed the determination of the cytotoxicity in fibroblasts, keratinocytes, and macrophages. According to the ISO 10993–5:2009 standard, a minimum viability of 70 % is considered a device as non-cytotoxic [51]. As shown in Fig. 6, the bactericidal concentration Br-CY5 (800 nM) was cytotoxic for the cellular lines tested, except for the fibroblasts (Fig. 6, left). However, when Br-CY5 was encapsulated in PLGA MPs, its cytotoxicity was significantly reduced exhibiting cell viability comparable to that of the untreated controls (Fig. 6, right). Therefore, the encapsulation of Br-CY5 in PLGA MPs, and their incorporation into PCL membranes, not only protects the PS from degradation but also reduces its cytotoxicity, allowing its use as a bactericidal agent that does not affect the eukaryotic cells tested.

4. Conclusions

This study explores the development of a light-responsive advanced wound dressing based on electrospun polymeric fibers decorated with cyanine-loaded polymeric microparticles (MPs), specifically designed for antimicrobial photodynamic therapy (aPDT). The incorporation of a brominated cyanine dye (Br-CY5) into PLGA microparticles and its subsequent integration into PCL electrospun fibers demonstrated significant antibacterial efficacy, presenting a promising approach for infection control in wound care.

At a concentration of 400 nM, the selected cyanine dye Br-CY5

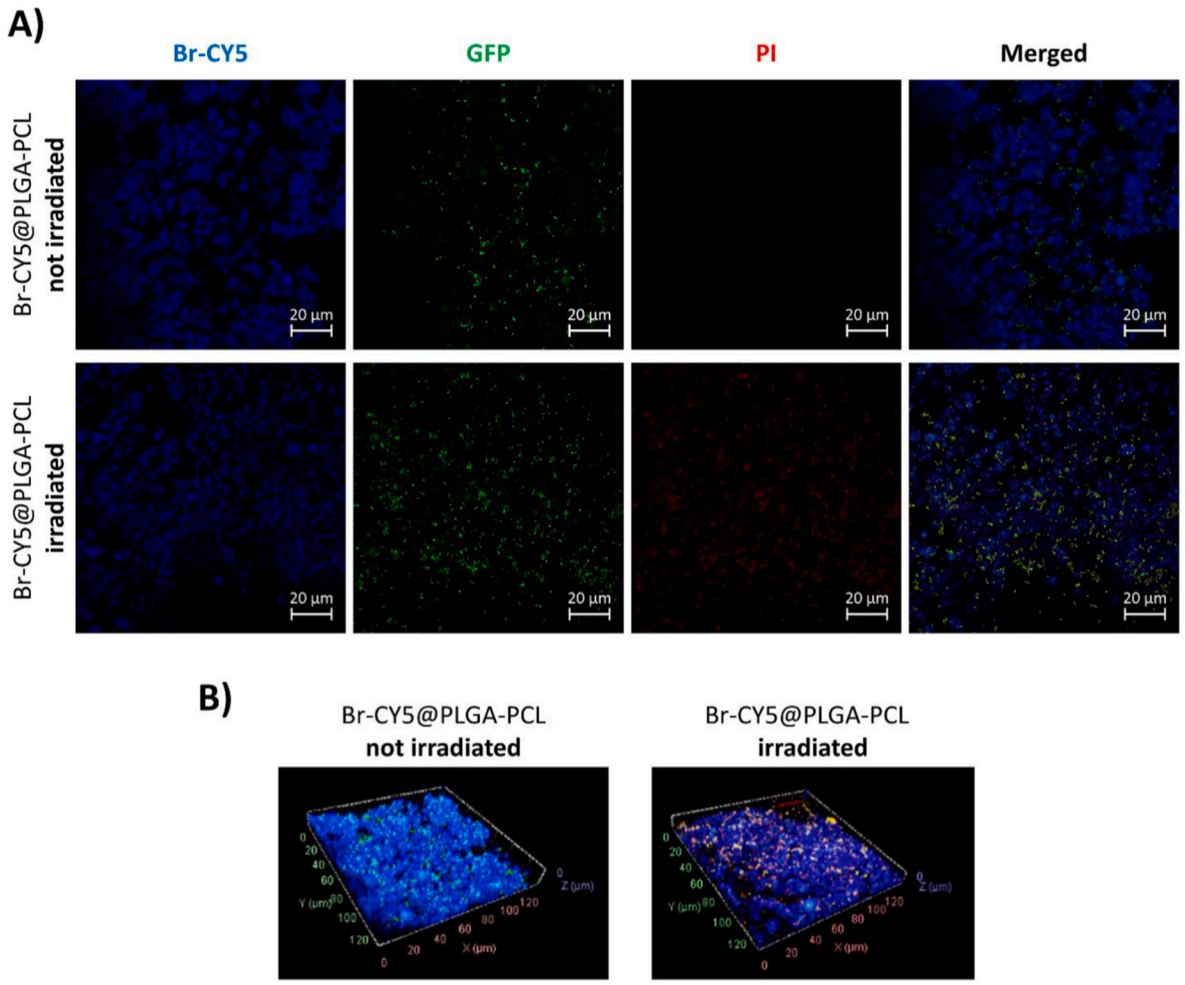

Fig. 5. Confocal fluorescent microscopy images: A) 2D visualization of Br-CY5@PLGA-PCL mats incubated with *S. aureus* expressing GFP without irradiation (top) and after irradiation at 17.4 mW/cm^2 for 15 min (bottom), B) orthogonal 3D projections visualization of Br-CY5@PLGA-PCL mats incubated with *S. aureus* expressing GFP without irradiation (left) and after irradiation at 17.4 mW/cm^2 for 15 min (right). Blue fluorescence corresponds to Br-CY5, GFP green fluorescence to GFP protein of viable *S. aureus* bacteria and red fluorescence to PI bound to the DNA of dead bacteria.

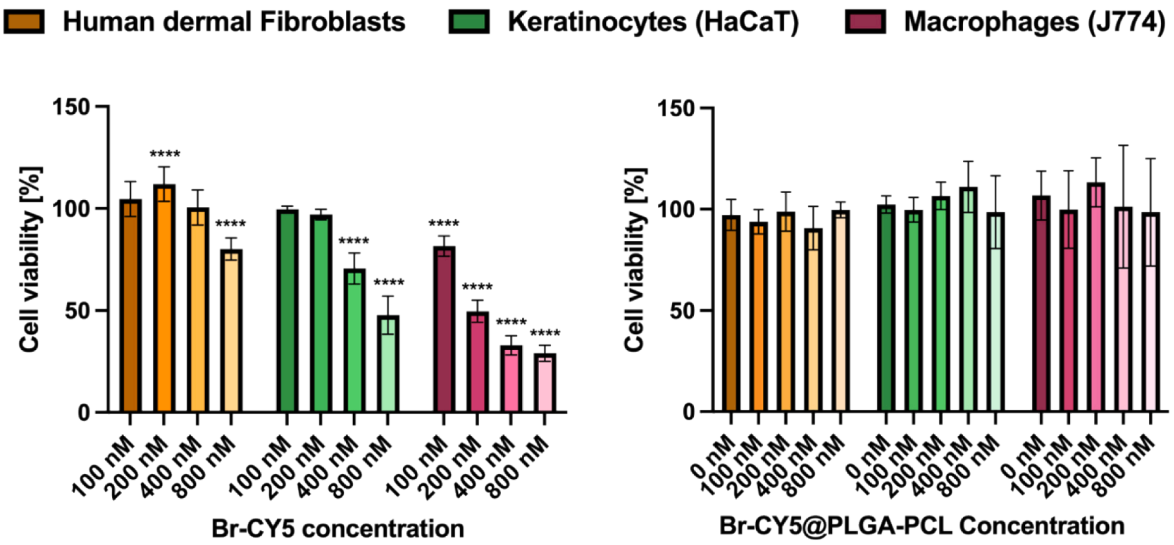

Fig. 6. *In vitro* cytotoxicity studies of Br-CY5 and the Br-CY5@PLGA-PCL system on different eukaryotic cell lines. Three experiments with 4 replicas were performed to obtain results as mean ± SD. Data were analyzed using GraphPad Prism 8 (GraphPad Software Inc., USA) by two-way ANOVA followed by multiple comparison tests. Statistical significance was defined as follows: *$p < 0.05$, **$p < 0.01$, ***$p < 0.001$, and ****$p < 0.0001$, comparing untreated control cells with treated cells.

achieved a remarkable 2.5-log reduction in bacterial growth, a higher reduction compared to the 5 μM threshold required for toluidine (used as standard) to exhibit antimicrobial efficacy. The use of extended irradiation at varying irradiances revealed a light-dose-dependent bacterial reduction, with 99.99 % eradication of *S. aureus* achieved after 15 min of irradiation at 17.4 mW/cm^2, offering a compelling solution for efficient aPDT applications. The investigation into the reactive oxygen species (ROS) production capacity of Br-CY5 highlighted its superior efficiency, surpassing even toluidine in generating ROS within the first 5 min of exposure. However, Br-CY5 showed photodegradation after 8 min of irradiation. To face this drawback and to design a wound dressing to treat bacterial infections, Br-CY5 has been incorporated into PLGA microparticles (MPs) and then deposited onto PCL nanofiber mats that allowed to protect the dye's photochemical integrity while ensuring stable release and enhanced efficacy. The morphological examination of the PCL nanofibers revealed a highly porous structure with a diameter of around 1 μm. After an optimization process, Br-CY5 loaded PLGA MPs with a size of 1 ± 0.21 μm were successfully and uniformly distributed on the surface of PCL nanofiber mats, to be potentially used as advanced wound dressings. With a high entrapment efficiency reaching a concentration of 1.2 μg of Br-CY5 per mg of Br-CY5-PLGA@PCL mat and consistent distribution of the loaded MPs, the developed nanofiber mats demonstrated a sustained release of the dye in 24 h and a substantial 3-log reduction in bacterial growth after 24 h of incubation and 15 min of irradiation, offering a promising approach for improving aPDT strategies. Overall, this study presents a novel, efficient, and stable material for targeted antimicrobial therapy, with strong potential for applications in infection control and wound healing.

CRediT authorship contribution statement

Degnet Melese Dereje: Writing – original draft, Methodology, Formal analysis. **Carlotta Pontremoli:** Writing – review & editing, Writing – original draft, Supervision, Investigation, Data curation, Conceptualization. **Cristina Yus:** Writing – review & editing, Writing – original draft, Supervision, Investigation, Data curation, Conceptualization. **Enrique Gámez:** Methodology, Investigation, Formal analysis. **Monica Paesa:** Methodology, Investigation, Formal analysis. **Gracia Mendoza:** Writing – review & editing, Supervision, Methodology, Conceptualization. **Manuel Arruebo:** Writing – review & editing, Writing – original draft, Supervision, Funding acquisition, Conceptualization. **Nadia Barbero:** Writing – review & editing, Supervision, Funding acquisition, Conceptualization.

Funding

This research was funded by "Grant for Internalization (GFI)", granted by the Department of Chemistry, University of Torino, Italy and by the Spanish Ministry of Science, Innovation and Universities grant nr. PID2023-146091OB-I00.

Declaration of competing interest

The authors declare that they have no known competing financial interests or personal relationships that could have appeared to influence the work reported in this paper.

Acknowledgements

M.P. acknowledges the support from Aragon regional government (Orden CUS/581/2020 and Orden CUS/803/202, respectively). G.M. gratefully acknowledges the support from the Miguel Servet Program (MS19/00092; Instituto de Salud Carlos III). D.M.D., C.P. and N.B. acknowledge support from the Project CH4.0 under the MUR program "Dipartimenti di Eccellenza 2023–2027" (CUP: D13C22003520001).

Appendix A. Supplementary data

Supplementary data to this article can be found online at https://doi.org/10.1016/j.mtchem.2025.103109.

Data availability

Data will be made available on request.

References

[1] S.R. Nussbaum, M.J. Carter, C.E. Fife, J. DaVanzo, R. Haught, M. Nusgart, D. Cartwright, An economic evaluation of the impact, cost, and medicare policy implications of chronic nonhealing wounds, Value Health 21 (2018) 27–32, https://doi.org/10.1016/j.jval.2017.07.007.

[2] M. Falcone, B. De Angelis, F. Pea, A. Scalise, S. Stefani, R. Tasinato, O. Zanetti, L. Dalla Paola, Challenges in the management of chronic wound infections, J. Glob. Antimicrob. Resist. 26 (2021) 140–147, https://doi.org/10.1016/j.jgar.2021.05.010.

[3] E. Gámez-Herrera, S. García-Salinas, S. Salido, M. Sancho-Albero, V. Andreu, M. Pérez, L. Luján, S. Irusta, M. Arruebo, G. Mendoza, Drug-eluting wound dressings having sustained release of antimicrobial compounds, Eur. J. Pharm. Biopharm. 152 (2020) 327–339, https://doi.org/10.1016/j.ejpb.2020.05.025.

[4] J. Dissemond, M. Augustin, S.A. Eming, T. Goerge, T. Horn, S. Karrer, H. Schumann, M. Stücker, Modern wound care – practical aspects of non-interventional topical treatment of patients with chronic wounds, JDDG J. der Deutschen Dermatol. Gesellschaft 12 (2014) 541–554, https://doi.org/10.1111/ddg.12351.

[5] Musharrat Jahan Prima, Masriana Hassan, Juhi Sharma, Novel approaches for combating antibiotic resistance in pathogenic bacteria, Microb Bioact 6 (2023), https://doi.org/10.25163/microbbioacts.619373.

[6] A. Stojadinovic, J.W. Carlson, G.S. Schultz, T.A. Davis, E.A. Elster, Topical advances in wound care, Gynecol. Oncol. 111 (2008) S70–S80, https://doi.org/10.1016/j.ygyno.2008.07.042.

[7] X. Ding, Q. Tang, Z. Xu, Y. Xu, H. Zhang, D. Zheng, S. Wang, Q. Tan, J. Maitz, P. K. Maitz, S. Yin, Y. Wang, J. Chen, Challenges and innovations in treating chronic and acute wound infections: from basic science to clinical practice, Burns Trauma 10 (2022), https://doi.org/10.1093/burnst/tkac014.

[8] M. Naghavi, S.E. Vollset, K.S. Ikuta, L.R. Swetschinski, A.P. Gray, E.E. Wool, G. Robles Aguilar, T. Mestrovic, G. Smith, C. Han, R.L. Hsu, J. Chalek, D.T. Araki, E. Chung, C. Raggi, A. Gershberg Hayoon, N. Davis Weaver, P.A. Lindstedt, A. E. Smith, U. Altay, N.V. Bhattacharjee, K. Giannakis, F. Fell, B. McManigal, N. Ekapirat, J.A. Mendes, T. Runghien, O. Srimokla, A. Abdelkader, S. Abd-Elsalam, R.G. Aboagye, H. Abolhassani, H. Abualruz, U. Abubakar, H. J. Abukhadijah, S. Aburuz, A. Abu-Zaid, S. Achalapong, I.Y. Addo, V. Adekanmbi, T.E. Adeyeoluwa, Q.E.S. Adnani, L.A. Adzigbli, M.S. Afzal, S. Afzal, A. Agodi, A. J. Ahlstrom, A. Ahmad, S. Ahmad, T. Ahmad, A. Ahmadi, A. Ahmed, H. Ahmed, I. Ahmed, M. Ahmed, S. Ahmed, S.A. Ahmed, M.A. Akkaif, S. Al Awaidy, Y. Al Thaher, S.O. Alalalmeh, M.T. AlBataineh, W.A. Aldhaleei, A.A.S. Al-Gheethi, N. B. Alhaji, A. Ali, L. Ali, S.S. Ali, W. Ali, K. Allel, S. Al-Marwani, A. Alrawashdeh, A. Altaf, A.B. Al-Tammemi, J.A. Al-Tawfiq, K.H. Alzoubi, W.A. Al-Zyoud, B. Amos, J.H. Amuasi, R. Ancuceanu, J.R. Andrews, A. Anil, I.A. Anuoluwa, S. Anvari, A. E. Anyasodor, G.L.C. Apostol, J. Arabloo, M. Arafat, A.Y. Aravkin, D. Areda, A. Aremu, A.A. Artamonov, E.A. Ashley, M.O. Asika, S.S. Athari, M.M.W. Atout, T. Awoke, S. Azadnajafabad, J.M. Azam, S. Aziz, A.Y. Azzam, M. Babaei, F.-X. Babin, M. Badar, A.A. Baig, M. Bajcetic, S. Baker, M. Bardhan, H.J. Barqawi, Z. Basharat, A. Basiru, M. Bastard, S. Basu, N.S. Bayleyegn, M.A. Belete, O.O. Bello, A. Beloukas, J.A. Berkley, A.S. Bhagavathula, S. Bhaskar, S.S. Bhuyan, J.A. Bielicki, N.I. Briko, C.S. Brown, A.J. Browne, D. Buonsenso, Y. Bustanji, C.G. Carvalheiro, C. A. Castañeda-Orjuela, M. Cenderadewi, J. Chadwick, S. Chakraborty, R. M. Chandika, S. Chandy, V. Chansamouth, V.K. Chattu, A.A. Chaudhary, P. R. Ching, H. Chopra, F.R. Chowdhury, D.-T. Chu, M. Chutiyami, N. Cruz-Martins, A.G. da Silva, O. Dadras, X. Dai, S.D. Darcho, S. Das, F.P. De la Hoz, D.M. Dekker, K. Dhama, D. Diaz, B.F.R. Dickson, S.G. Djorie, M. Dodangeh, S. Dohare, K. G. Dokova, O.P. Doshi, R.K. Dowou, H.L. Dsouza, S.J. Dunachie, A.M. Dziedzic, T. Eckmanns, A. Ed-Dra, A. Eftekharimehrabad, T.C. Ekundayo, I. El Sayed, M. Elhadi, W. El-Huneidi, C. Elias, S.J. Ellis, R. Elsheikh, I. Elsohaby, C. Eltaha, B. Eshrati, M. Eslami, D.W. Eyre, A.O. Fadaka, A.F. Fagbamigbe, A. Fahim, A. Fakhri-Demeshghieh, F.O. Fasina, M.M. Fasina, A. Fatehizadeh, N.A. Feasey, A. Feizkhah, G. Fekadu, F. Fischer, I. Fitriana, K.M. Forrest, C. Fortuna Rodrigues, J.E. Fuller, M.A. Gadanya, M. Gajdács, A.P. Gandhi, E.E. Garcia-Gallo, D.O. Garrett, R.K. Gautam, M.W. Gebregergis, M. Gebrehiwot, T.G. Gebremeskel, C. Geffers, L. Georgalis, R.M. Ghazy, M. Golechha, D. Golinelli, M. Gordon, S. Gulati, R. Das Gupta, S. Gupta, V.K. Gupta, A.D. Habteyohannes, S. Haller, H. Harapan, M. L. Harrison, A.I. Hasaballah, I. Hasan, R.S. Hasan, H. Hasani, A.H. Haselbeck, M. S. Hasnain, I.I. Hassan, S. Hassan, M.S. Hassan Zadeh Tabatabaei, K. Hayat, J. He, O.E. Hegazi, M. Heidari, K. Hezam, R. Holla, M. Holm, H. Hopkins, M.M. Hossain, M. Hosseinzadeh, S. Hostiuc, N.R. Hussein, L.D. Huy, E.D. Ibáñez-Prada, A. Ikiroma, I.M. Ilic, S.M.S. Islam, F. Ismail, N.E. Ismail, C.D. Iwu, C.J. Iwu-Jaja, A. Jafarzadeh, F. Jaiteh, R. Jalilzadeh Yengejeh, R.D.G. Jamora, J. Javidnia, T. Jawaid, A.W.J. Jenney, H.J. Jeon, M. Jokar, N. Jomehzadeh, T. Joo, N. Joseph, Z. Kamal, K.K. Kanmodi, R.S. Kantar, J.A. Kapisi, I.M. Karaye, Y.S. Khader, H. Khajuria, N. Khalid, F. Khamesipour, A. Khan, M.J. Khan, M.T. Khan, V. Khanal,

F.F. Khidri, J. Khubchandani, S. Khusuwan, M.S. Kim, A. Kisa, V.A. Korshunov, F. Krapp, R. Krumkamp, M. Kuddus, M. Kulimbet, D. Kumar, E.A.P. Kumaran, A. Kuttikkattu, H.H. Kyu, I. Landires, B.K. Lawal, T.T.T. Le, I.M. Lederer, M. Lee, S. W. Lee, A. Lepape, T.L. Lerango, V.S. Ligade, C. Lim, S.S. Lim, L.W. Limenh, C. Liu, X. Liu, X. Liu, M.J. Loftus, H.I.M. Amin, K.L. Maass, S.B. Maharaj, M.A. Mahmoud, P. Maikanti-Charalampous, O.M. Makram, K. Malhotra, A.A. Malik, G. D. Mandilara, F. Marks, B.A. Martinez-Guerra, M. Martorell, H. Masoumi-Asl, A. G. Mathioudakis, J. May, T.A. McHugh, J. Meiring, H.N. Meles, A. Melese, E. B. Melese, G. Minervini, N.S. Mohamed, S. Mohammed, S. Mohan, A.H. Mokdad, L. Monasta, A. Moodi Ghalibaf, C.E. Moore, Y. Moradi, E. Mossialos, V. Mougin, G. D. Mukoro, F. Mulita, B. Muller-Pebody, E. Murillo-Zamora, S. Musa, P. Musicha, L. A. Musila, S. Muthupandian, A.J. Nagarajan, P. Naghavi, F. Nainu, T.S. Nair, H.H. R. Najmuldeen, Z.S. Natto, J. Nauman, B.P. Nayak, G.T. Nchanji, P. Ndishimye, I. Negoi, R.I. Negoi, S.A. Nejadghaderi, Q.P. Nguyen, E.A. Noman, D.C. Nwakanma, S. O'Brien, T.J. Ochoa, I.A. Odetokun, O.A. Ogundijo, T.R. Ojo-Akosile, S.R. Okeke, O.C. Okonji, A.T. Olagunju, A. Olivas-Martinez, A.A. Olorukooba, P. Olwoch, K. I. Onyedibe, E. Ortiz-Brizuela, O. Osuolale, P. Ounchanum, O.T. Oyeyemi, M.P. P A, J.L. Paredes, R.R. Parikh, J. Patel, S. Patil, S. Pawar, A.Y. Peleg, P. Peprah, J. Perdigão, C. Perrone, I.-R. Petcu, K. Phommasone, Z.Z. Piracha, D. Poddighe, A. J. Pollard, R. Poluru, A. Ponce-De-Leon, J. Puvvula, F.N. Qamar, N.H. Qasim, C. D. Rafai, P. Raghav, L. Rahbarnia, F. Rahim, V. Rahimi-Movaghar, M. Rahman, M. A. Rahman, H. Ramadan, S.K. Ramasamy, P.S. Ramesh, P.W. Ramteke, R.K. Rana, U. Rani, M.-M. Rashidi, D. Rathish, S. Rattanavong, S. Rawaf, E.M.M. Redwan, L. F. Reyes, T. Roberts, J.V. Robotham, V.D. Rosenthal, A.G. Ross, N. Roy, K.E. Rudd, C.J. Sabet, B.A. Saddik, M.R. Saeb, U. Saeed, S. Saeedi Moghaddam, W. Saengchan, M. Safaei, A. Saghazadeh, N. Saheb Sharif-Askari, A. Sahebkar, S.S. Sahoo, M. Sahu, M. Saki, N. Salam, Z. Saleem, M.A. Saleh, Y.L. Samodra, A.M. Samy, A. Saravanan, M. Satpathy, A.E. Schumacher, M. Sedighi, S. Seekaew, M. Shafie, P. A. Shah, S. Shahid, M.J. Shahwan, S. Shakoor, N. Shalev, M.A. Shamim, M. A. Shamshirgaran, A. Shamsi, A. Sharifan, R.P. Shastry, M. Shetty, A. Shittu, S. Shrestha, E.E. Siddig, T. Sideroglou, J. Sifuentes-Osornio, L.M.L.R. Silva, E.A. F. Simões, A.J.H. Simpson, A. Singh, S. Singh, R. Sinto, S.S.M. Soliman, S. Soraneh, N. Stoesser, T.Z. Stoeva, C.K. Swain, L. Szarpak, S.S. T Y, S. Tabatabai, C. Tabche, Z. M.-A. Taha, K.-K. Tan, N. Tasak, N.Y. Tat, A. Thaiprakong, P. Thangaraju, C. C. Tigoi, K. Tiwari, M.R. Tovani-Palone, T.H. Tran, M. Tumurkhuu, P. Turner, A. J. Udoakang, A. Udoh, N. Ullah, S. Ullah, A.G. Vaithinathan, M. Valenti, T. Vos, H. T.L. Vu, Y. Waheed, A.S. Walker, J.L. Walson, T. Wangrangsimakul, K. G. Weerakoon, H.F.L. Wertheim, P.C.M. Williams, A.A. Wolde, T.M. Wozniak, F. Wu, Z. Wu, M.K.K. Yadav, S. Yaghoubi, Z.S. Yahaya, A. Yarahmadi, S. Yezli, Y. E. Yismaw, D.K. Yon, C.-W. Yuan, H. Yusuf, F. Zakham, G. Zamagni, H. Zhang, Z.-J. Zhang, M. Zielińska, A. Zumla, S.H.H. Zyoud, S.H. Zyoud, S.I. Hay, A. Stergachis, B. Sartorius, B.S. Cooper, C. Dolecek, C.J.L. Murray, Global burden of bacterial antimicrobial resistance 1990–2021: a systematic analysis with forecasts to 2050, Lancet 404 (2024) 1199–1226, https://doi.org/10.1016/S0140-6736(24)01867-1.

[9] F. Cieplik, D. Deng, W. Crielaard, W. Buchalla, E. Hellwig, A. Al-Ahmad, T. Maisch, Antimicrobial photodynamic therapy – what we know and what we don't, Crit. Rev. Microbiol. 44 (2018) 571–589, https://doi.org/10.1080/1040841X.2018.1467876.

[10] F. Cieplik, W. Buchalla, E. Hellwig, A. Al-Ahmad, K.A. Hiller, T. Maisch, L. Karygianni, Antimicrobial photodynamic therapy as an adjunct for treatment of deep carious lesions—A systematic review, Photodiagnosis Photodyn. Ther. 18 (2017) 54–62, https://doi.org/10.1016/j.pdpdt.2017.01.005.

[11] Y. Gilaberte, A. Rezusta, A. Juarranz, M.R. Hamblin, Editorial: antimicrobial photodynamic therapy: a new paradigm in the fight against infections, Front. Med. 8 (2021), https://doi.org/10.3389/fmed.2021.788888.

[12] H. Mahmoudi, A. Bahador, M. Pourhajibagher, M.Y. Alikhani, Antimicrobial photodynamic therapy: an effective alternative approach to control bacterial infections, J. Laser Med. Sci. 9 (2018) 154–160, https://doi.org/10.15171/jlms.2018.29.

[13] D.M. Dereje, C. Pontremoli, M.J. Moran Plata, S. Visentin, N. Barbero, Polymethine dyes for PDT: recent advances and perspectives to drive future applications, Photochem. Photobiol. Sci. (2022), https://doi.org/10.1007/s43630-022-00175-6.

[14] V.-N. Nguyen, Z. Zhao, B.Z. Tang, J. Yoon, Organic photosensitizers for antimicrobial phototherapy, Chem. Soc. Rev. 51 (2022) 3324–3340, https://doi.org/10.1039/D1CS00647A.

[15] J. Ghorbani, D. Rahban, S. Aghamiri, A. Teymouri, A. Bahador, Photosensitizers in antibacterial photodynamic therapy: an overview, Laser Ther. 27 (2018) 293–302, https://doi.org/10.5978/islsm.27_18-RA-01.

[16] M. Tim, Strategies to optimize photosensitizers for photodynamic inactivation of bacteria, J. Photochem. Photobiol., B 150 (2015) 2–10, https://doi.org/10.1016/j.jphotobiol.2015.05.010.

[17] S.J. Sharma, N. Sekar, Deep-red/NIR emitting coumarin derivatives - synthesis, photophysical properties, and biological applications, Dyes Pigments 202 (2022) 110306, https://doi.org/10.1016/j.dyepig.2022.110306.

[18] A.M. Smith, M.C. Mancini, S. Nie, Second window for in vivo imaging, Nat. Nanotechnol. 4 (2009) 710–711, https://doi.org/10.1038/nnano.2009.326.

[19] B.S. McGhie, J.R. Aldrich-Wright, Photoactive and luminescent transition metal complexes as anticancer agents: a guiding light in the search for new and improved cancer treatments, Biomedicines 10 (2022) 578, https://doi.org/10.3390/biomedicines10030578.

[20] L.A. Sordillo, S. Pratavieira, Y. Pu, K. Salas-Ramirez, L. Shi, L. Zhang, Y. Budansky, R.R. Alfano, in: R.R. Alfano, S.G. Demos (Eds.), Third Therapeutic Spectral Window for Deep Tissue Imaging, 2014 89400V, https://doi.org/10.1117/12.2040604.

[21] J.L. Bricks, A.D. Kachkovskii, Y.L. Slominskii, A.O. Gerasov, S.V. Popov, Molecular design of near infrared polymethine dyes: a review, Dyes Pigments 121 (2015) 238–255, https://doi.org/10.1016/j.dyepig.2015.05.016.

[22] N. Bordignon, M. Köber, G. Chinigò, C. Pontremoli, E. Sansone, G. Vargas-Nadal, M.J. Moran Plata, A. Fiorio Pla, N. Barbero, J. Morla-Folch, N. Ventosa, Quatsomes loaded with squaraine dye as an effective photosensitizer for photodynamic therapy, Pharmaceutics 15 (2023) 902, https://doi.org/10.3390/pharmaceutics15030902.

[23] D.M. Dereje, C. Pontremoli, A. García, S. Galliano, M. Colilla, B. González, M. Vallet-Regí, I. Izquierdo-Barba, N. Barbero, Poly Lactic-co-Glycolic acid (PLGA) loaded with a squaraine dye as photosensitizer for antimicrobial photodynamic therapy, Polymers (Basel) 16 (2024), https://doi.org/10.3390/polym16141962.

[24] S. Rojas-Buzo, C. Pontremoli, S. De Toni, K. Bondar, S. Galliano, H. Paja, B. Civalleri, A. Fiorio Pla, C. Barolo, F. Bonino, N. Barbero, Hafnium-based metal-organic framework nanosystems entrapping squaraines for efficient NIR-responsive photodynamic therapy, ACS Appl. Mater. Interfaces (2024), https://doi.org/10.1021/acsami.4c17018.

[25] C. Yus, T. Alejo, C. Quílez, S. Irusta, D. Velasco, M. Arruebo, V. Sebastian, Development of a hybrid CuS-ICG polymeric photosensitive vector and its application in antibacterial photodynamic therapy, Int. J. Pharm. 667 (2024) 124951, https://doi.org/10.1016/j.ijpharm.2024.124951.

[26] L. Miranda-Calderon, C. Yus, C. Remirez de Ganuza, M. Paesa, G. Landa, E. Tapia, E. Pérez, M. Perez, V. Sebastian, S. Irusta, G. Mendoza, M. Arruebo, Combinatorial wound dressings loaded with synergistic antibiotics in the treatment of chronic infected wounds, Chem. Eng. J. 476 (2023) 146679, https://doi.org/10.1016/j.cej.2023.146679.

[27] A.N. Severyukhina, N.V. Petrova, A.M. Yashchenok, D.N. Bratashov, K. Smuda, I. A. Mamonova, N.A. Yurasov, D.M. Puchinyan, R. Georgieva, H. Bäumler, A. Lapanje, D.A. Gorin, Light-induced antibacterial activity of electrospun chitosan-based material containing photosensitizer, Mater. Sci. Eng. C 70 (2017) 311–316, https://doi.org/10.1016/j.msec.2016.09.005.

[28] A. Contreras, M.J. Raxworthy, S. Wood, G. Tronci, Hydrolytic degradability, cell tolerance and On-Demand antibacterial effect of electrospun photodynamically active fibres, Pharmaceutics 12 (2020) 711, https://doi.org/10.3390/pharmaceutics12080711.

[29] E. Gámez, H. Elizondo-Castillo, J. Tascon, S. García-Salinas, N. Navascues, G. Mendoza, M. Arruebo, S. Irusta, Antibacterial effect of thymol loaded SBA-15 nanorods incorporated in PCL electrospun fibers, Nanomaterials 10 (2020) 616, https://doi.org/10.3390/nano10040616.

[30] S. García-Salinas, E. Gámez, J. Asín, R. de Miguel, V. Andreu, M. Sancho-Albero, G. Mendoza, S. Irusta, M. Arruebo, Efficiency of antimicrobial electrospun thymol-loaded polycaprolactone mats in vivo, ACS Appl. Bio Mater. 3 (2020) 3430–3439, https://doi.org/10.1021/acsabm.0c00419.

[31] E. Preis, T. Anders, J. Širc, R. Hobzova, A.-I. Cocarta, U. Bakowsky, J. Jedelská, Biocompatible indocyanine green loaded PLA nanofibers for in situ antimicrobial photodynamic therapy, Mater. Sci. Eng. C 115 (2020) 111068, https://doi.org/10.1016/j.msec.2020.111068.

[32] B. Gutberlet, E. Preis, V. Roschenko, U. Bakowsky, Photothermally controlled drug release of poly(d,l-lactide) nanofibers loaded with indocyanine green and curcumin for efficient antimicrobial photodynamic therapy, Pharmaceutics 15 (2023) 327, https://doi.org/10.3390/pharmaceutics15020327.

[33] K.B.R. Teodoro, A.D. Alvarenga, L.F. Rocha Oliveira, P.A. Marques Chagas, R. G. Lopes, R. da S. Andre, L.A. Mercante, F. Alves, M.D. Stringasci, H.H. Buzza, N. M. Inada, D.S. Correa, Fast fabrication of multifunctional PCL/curcumin nanofibrous membranes for wound dressings, ACS Appl. Bio Mater. 6 (2023) 2325–2337, https://doi.org/10.1021/acsabm.3c00177.

[34] B. Ciubini, S. Visentin, L. Serpe, R. Canaparo, A. Fin, N. Barbero, Design and synthesis of symmetrical pentamethine cyanine dyes as NIR photosensitizers for PDT, Dyes Pigments 160 (2019) 806–813, https://doi.org/10.1016/j.dyepig.2018.09.009.

[35] L. Serpe, S. Ellena, N. Barbero, F. Foglietta, F. Prandini, M.P. Gallo, R. Levi, C. Barolo, R. Canaparo, S. Visentin, Squaraines bearing halogenated moieties as anticancer photosensitizers: synthesis, characterization and biological evaluation, Eur. J. Med. Chem. 113 (2016) 187–197, https://doi.org/10.1016/j.ejmech.2016.02.035.

[36] C. Pontremoli, G. Chinigò, S. Galliano, M.J. Moran Plata, D.M. Dereje, E. Sansone, A. Gilardino, C. Barolo, A. Fiorio Pla, S. Visentin, N. Barbero, Photosensitizers for photodynamic therapy: structure-activity analysis of cyanine dyes through design of experiments, Dyes Pigments 210 (2023) 111047, https://doi.org/10.1016/j.dyepig.2022.111047.

[37] X. Huang, J. Lu, Y. An, M. Xu, X. Chen, C. Liu, X. Zhou, H. Shan, Y. Qian, M. Zhang, Electrospun PLGA/PCL nanofiber film loaded with LPA promotes full-layer wound healing by regulating the keratinocyte pyroptosis, ACS Appl. Mater. Interfaces 17 (2025) 20756–20767, https://doi.org/10.1021/acsami.4c22495.

[38] J. Aragón, S. Feoli, S. Irusta, G. Mendoza, Composite scaffold obtained by electrohydrodynamic technique for infection prevention and treatment in bone repair, Int. J. Pharm. 557 (2019) 162–169, https://doi.org/10.1016/j.ijpharm.2018.12.002.

[39] M. Paesa, C. Remirez de Ganuza, T. Alejo, C. Yus, S. Irusta, M. Arruebo, V. Sebastian, G. Mendoza, Elucidating the mechanisms of action of antibiotic-like ionic gold and biogenic gold nanoparticles against bacteria, J. Colloid Interface Sci. 633 (2023) 786–799, https://doi.org/10.1016/j.jcis.2022.11.138.

[40] E. Gámez, G. Mendoza, S. Salido, M. Arruebo, S. Irusta, Antimicrobial electrospun polycaprolactone-based wound dressings: an *in vitro* study about the importance of the direct contact to elicit bactericidal activity, Adv. Wound Care 8 (2019) 438–451, https://doi.org/10.1089/wound.2018.0893.

[41] B.C. Garms, H. Poli, D. Baggley, F.Y. Han, A.K. Whittaker, A. A, L. Grøndahl, Evaluating the effect of synthesis, isolation, and characterisation variables on reported particle size and dispersity of drug loaded PLGA nanoparticles, Mater. Adv. 2 (2021) 5657–5671, https://doi.org/10.1039/D1MA00410G.

[42] R. Atif, T. Salah Eldeen, L. Ahmed, I. Yahya, A. Omara, M. Eltayeb, Study the using of nanoparticles as drug delivery system based on mathematical models for controlled release. www.ijltemas, 2019.
[43] X. Xu, B. Liu, H. Wu, Y. Zhang, X. Tian, J. Tian, T. Liu, Poly Lactic-co-Glycolic acid-coated toluidine blue nanoparticles for the antibacterial therapy of wounds, Nanomaterials 11 (2021) 3394, https://doi.org/10.3390/nano11123394.
[44] Y. Yang, T. Tang, B. Liu, J. Tian, H. Wu, Z. Liu, Z. Liu, L. Zhang, H. Bao, T. Liu, TB@PLGA nanoparticles for photodynamic/photothermal combined cancer therapy with single near-infrared irradiation, Int. J. Nanomed. 16 (2021) 4863–4871, https://doi.org/10.2147/IJN.S304713.
[45] D.M. Dereje, A. García, C. Pontremoli, B. González, M. Colilla, M. Vallet-Regí, I. Izquierdo-Barba, N. Barbero, Squaraine-loaded mesoporous silica nanoparticles for antimicrobial photodynamic therapy against bacterial infection, Microporous Mesoporous Mater. 372 (2024) 113096, https://doi.org/10.1016/j.micromeso.2024.113096.
[46] H.E. ElZorkany, T. Youssef, M.B. Mohamed, R.M. Amin, Photothermal versus photodynamic treatment for the inactivation of the bacteria Escherichia coli and bacillus cereus: an in vitro study, Photodiagnosis Photodyn. Ther. 27 (2019) 317–326, https://doi.org/10.1016/j.pdpdt.2019.06.020.
[47] D. Park, E.J. Choi, K.-Y. Weon, W. Lee, S.H. Lee, J.-S. Choi, G.H. Park, B. Lee, M. R. Byun, K. Baek, J.W. Choi, Non-invasive photodynamic therapy against -Periodontitis-causing bacteria, Sci. Rep. 9 (2019) 8248, https://doi.org/10.1038/s41598-019-44498-4.
[48] N. Izquierdo, E. Gamez, T. Alejo, G. Mendoza, M. Arruebo, Antimicrobial photodynamic therapy using encapsulated protoporphyrin IX for the treatment of bacterial pathogens, Materials 17 (2024) 1717, https://doi.org/10.3390/ma17081717.
[49] L. Han, Y. Chen, J. Niu, L. Peng, Z. Mao, C. Gao, Encapsulation of a photosensitizer into cell membrane capsules for photodynamic therapy, RSC Adv. 6 (2016) 37212–37220, https://doi.org/10.1039/C6RA07480D.
[50] K. Löw, T. Knobloch, S. Wagner, A. Wiehe, A. Engel, K. Langer, H. von Briesen, Comparison of intracellular accumulation and cytotoxicity of free *m* THPC and *m* THPC-Loaded PLGA nanoparticles in human colon carcinoma cells, Nanotechnology 22 (2011) 245102, https://doi.org/10.1088/0957-4484/22/24/245102.
[51] https://www.iso.org/standard/36406.html, (n.d.).